

An electrochemical preparation of bismuth nanoparticles by reduction of bismuth oxide nanoparticles and their application as an environmental sensor

Gil Ho Hwang^a, Won Kyu Han^a, So Jin Kim^a, Seok Jun Hong^a, Joon Shik Park^b, Hyun Joon Park^a and Sung Goon Kang^{a,*}

^aDivision of Materials Science and Engineering, Hanyang University, Seoul 133-791, Korea

^bNano-mechatronics Research Center, KETI, Kyunggi 463-816, Korea

Bismuth nanoparticles were prepared by electrochemical reduction of bismuth oxide nanoparticles. Bismuth nitrate ($\text{Bi}(\text{NO}_3)_3 \cdot 5\text{H}_2\text{O}$) and ammonium hydroxide (NH_4OH) were used as starting materials and precipitant to synthesize bismuth hydroxide. After decomposition of bismuth hydroxide at 800°C , spherical bismuth oxide nanoparticles with a diameter of 200 nm were obtained. Bismuth oxide nanoparticles were electrochemically reduced to bismuth nanoparticles below -1.0 V (vs. SCE) in a 0.1 M KOH solution. The morphology and structure of the nanoparticles were analyzed with a scanning electron microscope (SEM), X-ray photoelectron spectroscopy (XPS) and X-ray diffraction (XRD). The bismuth nanoparticles prepared were applied for the simultaneous determination of lead and cadmium by square wave anodic stripping voltammetry. Screen-printed bismuth nanoparticle electrodes presented well-defined, reproducible and sharp stripping signals.

Key words: Bismuth oxide nanoparticles, Bismuth nanoparticles, Electrochemical reduction, Electrochemical sensor

Introduction

Bismuth has gained much attention in recent years for pharmaceutical and metallurgical additives [1-3]. In particular, bismuth is suggested as an alternative to mercury for an environmental sensor. The advantageous analytical properties of bismuth are attributed to its fused alloy formation with different metals [4-6]. Semimetal bismuth, which has a highly anisotropic Fermi surface, low conduction band effective mass and high electron mobility, is of great interest because of its size-induced semimetal to semiconductor transition [7-10]. When the crystallite size is decreased to the nano-scale, semimetal bismuth is converted to a semiconductor due to a quantum confinement effect, and this makes bismuth nanoparticles especially useful for optoelectronic and thermoelectric applications [11].

In general, bismuth nanoparticles are synthesized by a thermal plasma method, aerosol quenching, electron beam irradiation and laser ablation techniques [12-14]. However, these methods are inappropriate and impractical for the mass production of nanoparticles.

In this study, we obtained bismuth nanoparticles using a simple two-step procedure: the first step was the preparation of bismuth oxide nanoparticles via precipitation using bismuth nitrate in ammonium hydroxide, the second step was the electrochemical reduction of bismuth oxide nanoparticles in an alkaline solution. Triangular bismuth nanoparticles were

obtained by electrochemical reduction in a 0.1 M KOH solution. The morphology, size and structure of the bismuth nanoparticles were analyzed by a scanning electron microscope (SEM), X-ray photoelectron spectroscopy (XPS) and X-ray diffraction (XRD). The bismuth nanoparticles prepared were evaluated for the electrochemical analysis of lead and cadmium and their stripping responses were compared with commercial bismuth particles.

Experimental

Bismuth nanoparticles preparation

Bismuth nitrate ($\text{Bi}(\text{NO}_3)_3 \cdot 5\text{H}_2\text{O}$) was used as the starting material and ammonium hydroxide (NH_4OH) was used as the precipitant. To precipitate bismuth as a hydroxide, 0.1 M bismuth nitrate was dissolved in 1 M nitric acid, and 2 M ammonium hydroxide was added using a diaphragm pump at the rate of 5 ml/minute until the $\text{pH} = 12$. The hydrated bismuth hydroxide was washed with distilled water and ethanol (in a ratio of 3 : 2) and filtered with a 0.1 μm membrane. The precipitated bismuth hydroxide was oven-dried at 80°C for 24 h and then decomposed to bismuth oxide at 800°C for 2 h. To fabricate bismuth nanoparticles, a carbon container filled with bismuth oxide nanoparticles, was immersed in a 0.1 M KOH solution and a copper wire was connected to it. A potential of -1.2 V (vs. SCE) for 10 minutes was applied for the reduction of the bismuth oxide nanoparticles.

Electrochemical sensor preparation

Bismuth paste was prepared by mixing with a binder (SJ-52-1, Sungji Tech) using a pestle and mortar. Silver

*Corresponding author:
Tel : +82-2-2220-0404
Fax: +82-2-2296-4560
E-mail: sgkang@hanyang.ac.kr

and epoxy paste were used to form the metallic connection and insulating layer, respectively. Bismuth paste which served as a working electrode was formed onto the silver layer. Also the epoxy paste was printed except for the silver electrical connection and sensing area (3 mm diameter disk). Each baking step was performed at 130 °C for 30 minutes.

Stripping voltammetry

Stripping voltammetry was carried out in 0.1 M acetate buffer (pH 4.5). A preconcentration potential of -1.0 V (vs. SCE) was applied to the working electrode under stirring conditions. The stirring was stopped and after 10 s equilibration time, and the square wave anodic stripping voltammograms were recorded between -1.0 V to 0 V (frequency: 50 Hz, pulse height: 50 mV, step increment: 5 mV).

Results and Discussion

Bismuth oxide nanoparticles

Fig. 1 shows the spherical bismuth oxide nanoparticles, which were obtained from ammonium hydroxide as the precipitant. It is obvious that the product consists of partially agglomerated spherical nanoparticles with a diameter of 200-300 nm. The starting material, precipitant, reaction temperature, time and surfactant influenced the shape and size of bismuth oxide [15]. For example, Xiong *et al.* synthesized hand-like bismuth oxide using bismuth nitrate and sodium hydroxide [16]. Yang *et al.* synthesized bismuth oxide needles using bismuth hydroxide and potassium hydroxide [17]. In general, it is known that the addition of OH^- ions induces anisotropic growth towards a preferential direction and affects the formation of needle-shaped bismuth oxide [18]. However, the presence of OH^- ions could form spherical bismuth oxide as shown in Fig. 1 and reported by Li [19].

Bismuth nanoparticles

Cyclic voltammogram of bismuth oxide was carried out with a conventional three electrode cell in a 0.1 M KOH solution (Fig. 2). The bismuth oxide had two strong reduction

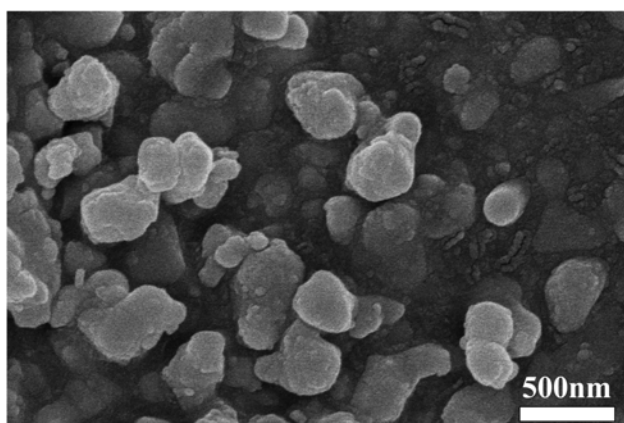


Fig. 1. SEM image of bismuth oxide nanoparticles prepared from NH_4OH .

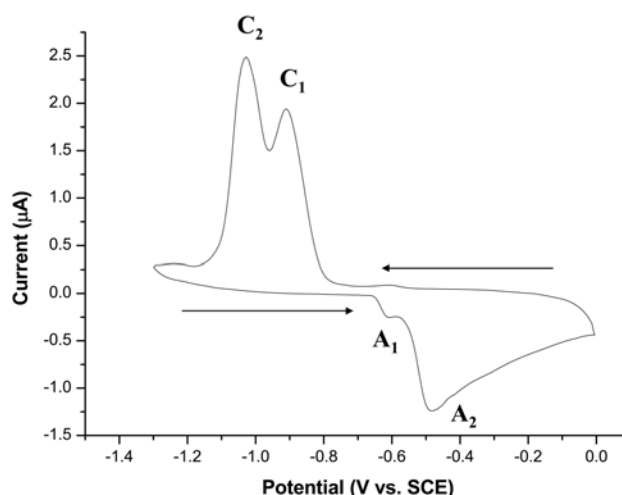
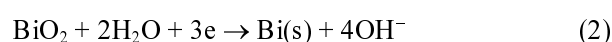
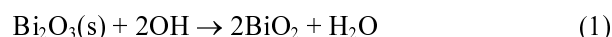


Fig. 2. Cyclic voltammogram of bismuth oxide nanoparticles in a 0.1 M KOH solution. Scan rate: 10 mV/s.

peaks observed at -0.9 V and -1.0 V (vs. SCE). In an alkaline solution, bismuth oxide makes a chemical reaction with OH^- ions (Eq. 1) and the following electrochemical reduction of BiO_2^- occurs at -0.9 V (Eq. 2) [20]:



The other reduction peak observed at -1.0 V was related to bismuth metal formation:



These results indicate that bismuth oxide nanoparticles were electrochemically converted to bismuth nanoparticles below -1.0 V. Thus, a potential of -1.2 V for 10 minutes was chosen for the reduction of the bismuth oxide nanoparticles. With an increase of reduction time, yellow-colored bismuth oxide nanoparticles darkened gradually and finally became black-colored bismuth nanoparticles.

XPS spectra of the bismuth oxide nanoparticles and bismuth nanoparticles were obtained and are shown in Fig. 3. Two asymmetrical peaks observed at 158.6 eV and 163.8 eV correspond to $\text{Bi } 4f_{7/2}$ and $\text{Bi } 4f_{5/2}$ of bismuth oxide [21, 22]. After the electrochemical reduction of bismuth oxide, new peaks were observed at 156.6 eV and 161.8 eV. The binding energies of the new peaks were consistent with Bi 4f spectra for the bismuth metal [23]. The $\text{Bi } 4f_{7/2}$ peak at 156.6 eV corresponds to Bi^0 and the signal at 158.6 eV is assigned to Bi^{3+} , which are in agreement with the XPS analysis of Ar^+ -sputtered bismuth oxide [24]. The shoulders at the higher binding energy side of the Bi 4f peaks are ascribed to the inevitable bismuth oxide formation during sample preparation for XPS analysis.

The XRD patterns of bismuth oxide nanoparticles and bismuth nanoparticles are displayed in Fig. 4. Bismuth oxide nanoparticles were of a monoclinic structure (JCPDS File No. 76-1730), and a residual bismuth hydroxide was

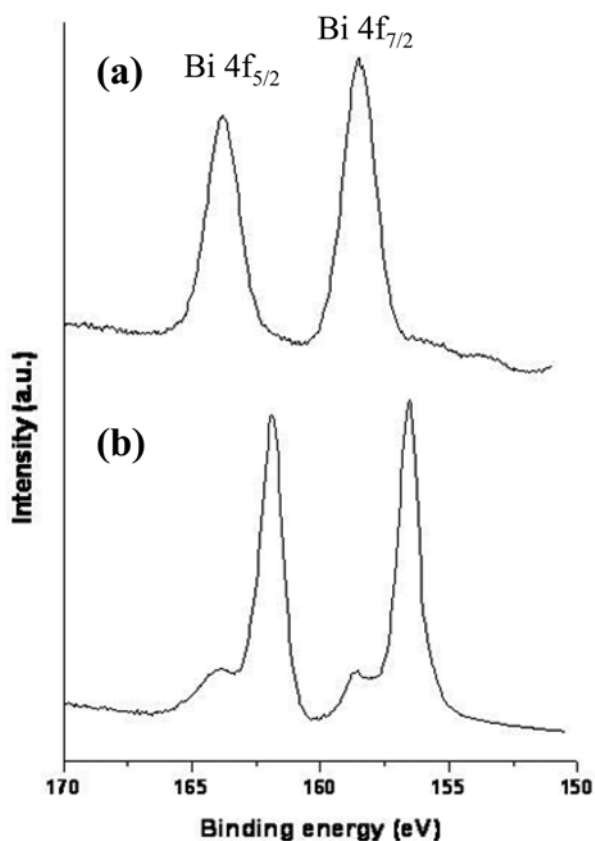


Fig. 3. XPS spectra of bismuth oxide nanoparticles before (a) and after (b) electrochemical reduction.

also observed (JCPDS File No. 01-0898). After the electrochemical reduction, all diffraction peaks of the XRD pattern were assigned to the rhombohedral bismuth phase (JCPDS File No. 85-1329), indicating that bismuth oxide nanoparticles and residual bismuth hydroxide were completely reduced to bismuth nanoparticles (Fig. 4(b)). From the XPS and XRD analyses, it could be concluded that bismuth oxide nanoparticles were successfully reduced to bismuth metal during the electrochemical reduction procedure.

A SEM image of bismuth nanoparticles is displayed in Fig. 5. While bismuth oxide nanoparticles formed soft agglomerates, bismuth nanoparticles were highly agglomerated after the electrochemical reduction. However, discrete nanoparticles were clearly observed and the size of each nanoparticle was not much different from that of the bismuth oxide nanoparticles. Although some other shapes were observed, the main morphology of the product was triangular. Fu *et al.* suggested a possible mechanism for the growing process of triangular bismuth [25]. High index crystallographic planes on a spherical single crystalline bismuth particle resulted in a higher surface energy. For an increase of the portion of low-index planes, facets tend to form on the particle surface. Growth rates of the different faces were quite different and the particles could grow towards a preferential direction with the influence of various factors. They reported that a low growth rate on (001) planes resulted in the formation of triangular plates.

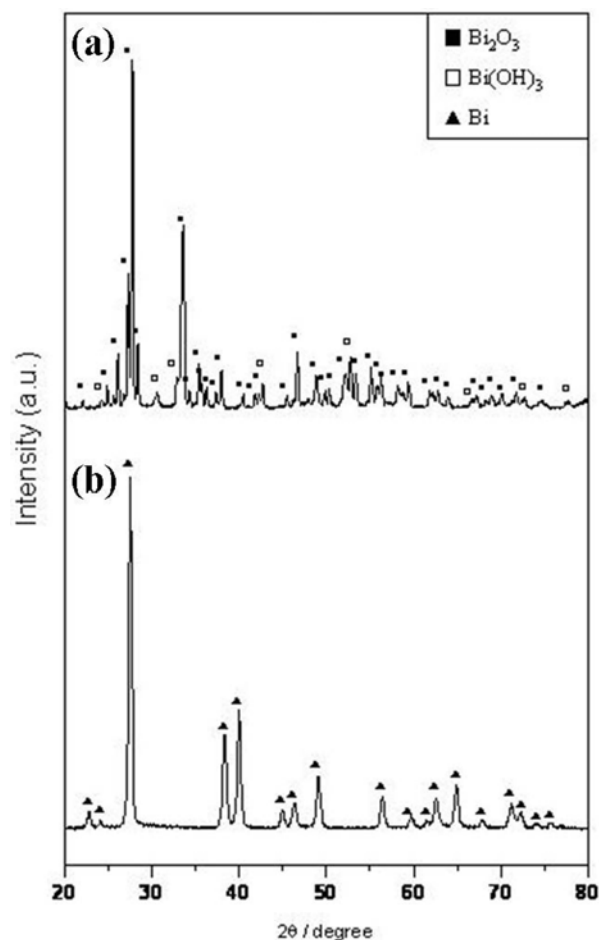


Fig. 4. XRD patterns of bismuth oxide nanoparticles (a) and bismuth nanoparticles (b) prepared from NH₄OH.

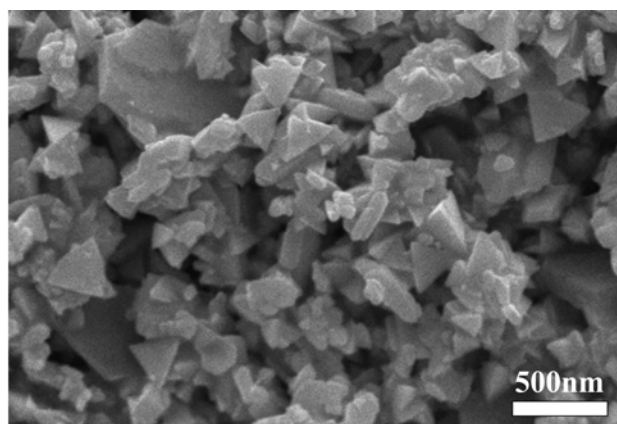


Fig. 5. SEM images of bismuth nanoparticles prepared from NH₄OH.

Application for environmental sensor

Stripping voltammograms of different bismuth electrodes are illustrated in Fig. 5. The average particle size of the commercial bismuth particles was 150 μm. Stripping voltammograms were obtained in 0.1 M acetate buffer solution (pH 4.5) containing 100 μg/l of lead and cadmium. The bismuth electrode prepared

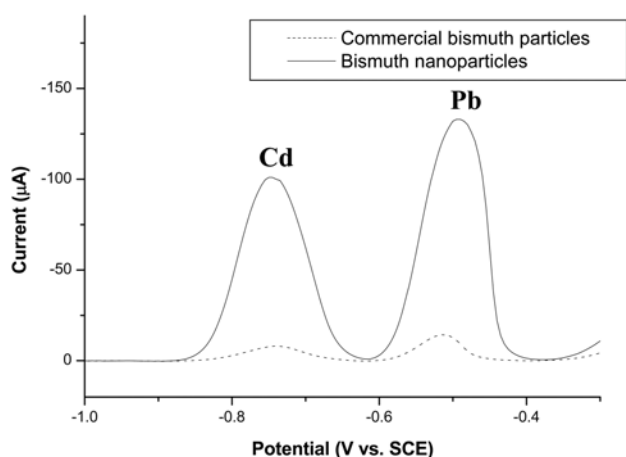


Fig. 6. Anodic stripping voltammograms of 100 $\mu\text{g/l}$ lead and cadmium at a bismuth electrode prepared from bismuth nanoparticles and commercial bismuth particles. Supporting electrolyte: 0.1 M acetate buffer (pH 4.5); deposition potential: -1.0 V; deposition time: 300 s; frequency: 50 Hz; pulse height: 50 mV; step increment: 5 mV.

from nanosized particles exhibited a sharper and the higher stripping response than that with the commercial particles. The stripping responses of bismuth nanoparticles were 10 times higher than those of commercial bismuth particles. It is considered that the increased surface area of the bismuth nanoparticles lead to the larger quantities of active sites, which means that more heavy metals could be deposited on the electrode. This increase of surface area resulted in an enhancement of the sensitivity of the bismuth nanoparticles. However, they exhibited no differences in hydrogen evolution potential and bismuth oxidation potential. A series of stripping voltammograms are shown in Fig. 7. The inset shows the calibration plot of

lead and cadmium. Each point on these curves is the mean values for 5 repeated measurements. The peak current increases linearly with the metal concentration with a slope of $0.59 \mu\text{A}/\mu\text{g l}^{-1}$ and $0.55 \mu\text{A}/\mu\text{g l}^{-1}$ for lead and cadmium (correlation coefficients: 0.999 for lead and for cadmium).

Conclusions

Bismuth oxide nanoparticles were synthesized from bismuth nitrate and ammonium hydroxide, and an electrochemical reduction method was applied for the preparation of bismuth nanoparticles. Monoclinic bismuth oxide nanoparticles and residual bismuth hydroxide were successfully converted to rhombohedral bismuth nanoparticles after the electrochemical reduction. The shape of the spherical bismuth oxide nanoparticles was transformed to triangles without a change in their size. A possible mechanism for the triangular bismuth was suggested by Fu *et al.* However, it is not obvious that this mechanism can be applied for the electrochemical reduction procedure. Thus, further effort is necessary to explain an obvious mechanism. An electrochemical sensor prepared with nanosized bismuth particles showed well-defined and sharp stripping responses for the determination of lead and cadmium. This excellent performance was attributed to an increase of the surface area, which means there are more active sites for the deposition of heavy metals.

Acknowledgements

This research was supported by Hanyang Fusion Materials Program funded by Ministry of Education, Science and Technology, Korea.

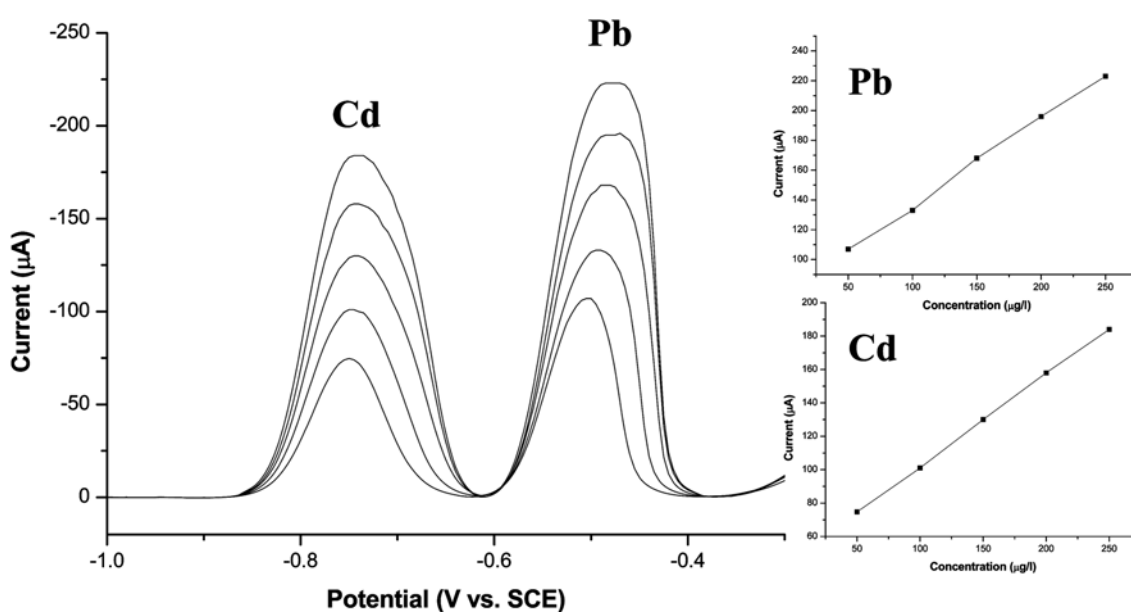


Fig. 7. A series of voltammograms for simultaneous determination of lead and cadmium obtained with a bismuth electrode prepared with bismuth nanoparticles. Other conditions as in Fig. 6.

References

1. V. Rodilla, A.T. Miles, W. Jenner and G.M. Hawksworth, *Chem.-Biol. Interact.* 115 (1998) 71-83.
2. H. Sun, H. Li, I. Harvey and P.J. Sadler, *J. Biol. Chem.* 274 (1999) 29094-29101.
3. 0H. Guo, Y. Li, P. Xiao and N. He, *Anal. Chim. Acta* 534 (2005) 143-147.
4. J. Wang, D. Lu, S. Thongngamdee, Y. Lin and O.A. Sadik, *Talanta* 69 (2006) 914-917.
5. S.B. Hocevar, B. Ogorevc, J. Wang and B. Pihlar, *Electroanalysis* 14 (2002) 1707-1712.
6. G. Kefala, A. Economou and M. Sofoniou, *Talanta* 68 (2006) 1013-1019.
7. J. Wang, X. Wang, Q. Peng and Y. Li, *Inorg. Chem.* 43 (2004) 7552-7556.
8. X.Y. Liu, J.H. Zeng, S.Y. Zhang, R.B. Zheng, X.M. Liu and Y.T. Qian, *Chem. Phys. Lett.* 374 (2003) 348-352.
9. G.G. Briand, N. Burford, M.D. Eelman, N. Aumeerally, L. Chen, T.S. Cameron and K.N. Robertson, *Inorg. Chem.* 43 (2004) 6495-6500.
10. Y.M. Lin, S.B. Cronin, J.Y. Ying, M.S. Dresselhaus and J.P. Heremans, *Appl. Phys. Lett.* 76 (2000) 3944-3946.
11. C.A. Hoffman, J.R. Meyer, F.J. Bartoli, A.D. Venere, X.J. Yi, C.L. Hou, H.C. Wang and J.B. Ketterson, *Phys. Rev. B* 48 (1993) 11431-11434.
12. L. Wang, Z.L. Cui and Z.K. Zhang, *Surf. Coat. Technol.* 201 (2007) 5330-5332.
13. K. Wegner, B. Walker and S.E. Pratsinis, *J. Aerosol. Sci.* 31 (2000) 214-215.
14. S.H. Kim, Y.S. Choi, K.H. Kang and S.I. Yang, *J. Alloy. Compd.* 427 (2007) 330-332.
15. M. Gotic, S. Popovic and S. Music, *Mater. Lett.* 61 (2007) 709-714.
16. Y. Xiong, M. Wu, J. Ye and Q. Chen, *Mater. Lett.* 62 (2008) 1165-1168.
17. Q. Yang, Y. Li, Q. Yin, P. Wang and Y. Cheng, *Mater. Lett.* 55 (2002) 46-49.
18. G. Dell'Agli, A. Colantuono and G. Mascolo, *Solid State Ion.* 123 (1999) 87-94.
19. W. Li, *Mater. Chem. Phys.* 99 (2006) 174-180.
20. A.M. Espinosa, M.T. San Jose, M.L. Tascon, M.D. Vazquez and P.S. Batanero, *Electrochim. Acta* 36 (1991) 1561-1571.
21. W. Xiaohong, Q. Wei and H. Weidong, *J. Mol. Catal. A-Chem.* 261 (2007) 167-171.
22. C. Hinnen, C.N. Van Huong and P. Marcus, *J. Electron Spectrosc. Relat. Phenom.* 73 (1995) 293-304.
23. I.G. Casella and M. Contursi, *Electrochim. Acta* 52 (2006) 649-657.
24. K. Uchida and A. Ayame, *Surf. Sci.* 357 (1996) 170-175.
25. R. Fu, S. Xu, Y. Lu and J. Zhu, *Cryst. Growth Des.* 5 (2007) 1379-1385.